RSC Advances

PAPER

View Article Online
View Journal | View Issue

Cite this: *RSC Adv.*, 2022, **12**, 23860

Preparation and characterization of lauric acid–stearic acid/expanded perlite as a composite phase change material

Xuying Liu, Yunchao Zhao, * Zhixuan Fan, Yu Shi and Dahua Jiang

Received 11th April 2022
Accepted 9th August 2022

DOI: 10.1039/d2ra02345h

rsc.li/rsc-advances

Rapid energy consumption stimulates the development of energy-saving materials. In this work, the L–S eutectic mixture used as a PCM was compounded with EP *via* vacuum adsorption to synthesize LS/EP CPCM. The maximum mass adsorption rate of EP on L–S is determined to be 70% *via* leakage experiments. The microscopic morphology, chemical, and crystal structure were characterized using scanning electron microscopy (SEM), Fourier transform infrared spectroscopy (FT-IR), and X-ray diffraction (XRD), respectively. The phase change properties were measured by differential scanning calorimetry (DSC). The melting temperature of LS/EP is 37.79 °C, with a latent heat of 126.05 J g^{-1}, and it has a crystallinity of over 90%. The thermal decomposition was evaluated by TGA. The initial decomposition temperature is 132.20 °C for LS/EP. In addition, the results of accelerated phase change cycling experiments showed that LS/EP CPCM has good reliability.

1. Introduction

In recent years, various non-renewable energy sources have been over-exploited, and global carbon emissions have increased dramatically.[1,2] Energy and environmental issues are deeply troubling people and governments around the world. In September 2020, the Chinese government announced that China's carbon dioxide emissions will peak by 2030 and China will become carbon neutral by 2060. In 2018, the energy consumption of China's buildings during operation was 1 billion tce, accounting for 21.7% of China's total energy consumption. In addition, the carbon emissions of the building operation stage are 2.11 billion tCO_2, accounting for 21.9% of China's carbon emissions.[3] Of these, HVAC systems are responsible for most of the energy consumption and carbon emissions. Therefore, the development of new energy-saving building materials is of great significance for energy saving and emissions reduction.

Phase change materials (PCMs), a latent heat storage medium, can absorb or release large amounts of latent heat during melting or solidification.[4,5] New building materials used in thermal storage and insulation are prepared by compounding PCM with traditional building materials, which can effectively reduce building energy consumption and adjust the indoor environment due to the high heat capacity characteristics of PCM.[6–10] Currently, the commonly used PCMs in the cryogenic field are inorganic hydrated salts and organic PCMs. Subcooling and phase separation of inorganic hydrated salts make them unsuitable for the use in building PCMs.[11,12] In contrast, organic PCMs do not have these disadvantages.[13,14] In addition, fatty acids in organic PCMs have the advantages of excellent thermal storage properties, good thermal stability, and weak chemical activity,[15] which make them a preferable choice for construction PCMs. However, fatty acids have a single melting point and leakage problems. To overcome these drawbacks, domestic and foreign scholars usually use binary and multiple eutectics to regulate the melting point and porous material adsorption to avoid leakage. For instance, Du[16] synthesized a capric acid–palmitic acid–stearic acid/expanded graphite composite by vacuum adsorption, where the CA : PA : SA mass ratio was 74.7 : 17 : 8.3, corresponding to a phase change temperature and latent heat of 25.39 °C and 140.22 J g^{-1}, respectively. In addition, Du[16] demonstrated by electron microscopy and leakage experiments that the porous carrier EG can effectively inhibit the leakage of fatty acids. Ramírez[17] investigated the maximum adsorption rates of CA–MA, LA–MA, and PA–SA in the same inorganic porous material and compared the thermal properties of the three composites. He[18] prepared a LA–MA/EG composite from LA, MA, and EG, and thermal cycling experiments showed that the material has good thermal cycling stability.

Selection of the adsorption carrier is a key part of composite preparation. At present, the commonly used porous adsorbent materials are porous metal-based,[19,20] porous carbon-based,[21,22] and porous mineral-based.[23,24] Compared to the other two porous materials, porous minerals are more suitable for building energy efficiency because of their characteristics, such as being cheaper and easier to access.[25,26] Expanded perlite (EP), a porous mineral, is characterized by large specific surface area,

School of Civil and Surveying Engineering, Jiangxi University of Science and Technology, Ganzhou 341000, Jiangxi Province, China. E-mail: yczhao@jxust.edu.cn

strong fire resistance, moderate hole size, low moisture retention, and a very low density.[27–30] Furthermore, it is an environmentally safe building material that is abundant in Chinese markets. Sari[31] synthesized a composite phase change material (CPCM) with a mass fraction of 55% capric acid by vacuum adsorption of capric acid (CA) on EP. In addition, the test results show that the thermal performance parameters of the synthesized CPCM are suitable for the field of building energy saving. Bian[27] prepared an expanded perlite aerogel that can adsorb twice its own mass of CA–SA while exhibiting good thermal and chemical properties. Therefore, EP is an appropriate and cost-effective option for synthesizing energy-efficient CPCMs for buildings.

This work aims to synthesize a novel CPCM for use in tropical and subtropical regions. Phase change processes include heat absorption and exothermic processes, and they interact with each other. We must choose a PCM with a high phase change temperature so that the stored heat can be released at night. Therefore, lauric acid (LA) with a high phase change temperature and stearic acid (SA) with the highest latent heat among fatty acids are used to synthesize a L–S eutectic PCM suitable for tropical and subtropical regions. Unlike many works, the use of low thermal conductivity EP as a support material to further enhance the thermal insulation is in response to the climatic characteristics of tropical and subtropical regions. To accurately determine the adsorption rate of EP to L–S, a series of CPCMs with different mass fractions of L–S were prepared. We use numerical (weighing mass loss) and sensory analysis (leak traces on filter paper are observed) methods to jointly determine the optimal adsorption rate. Moreover, under the optimal adsorption rate, the crystal and chemical structures, microscopic morphology, phase change performance parameters, thermal stability and reliability of the CPCM were analyzed and characterized.

2. Materials and methods

2.1 Materials

LA was purchased from Shandong Youshuo Composite Material Engineering Co. SA was provided by Sinopharm Chemical Reagent Co. EP was obtained from Xinyang expanded perlite factory in China, with a particle size of 70–90 mesh.

2.2 Purification of expanded perlite

First, the expanded perlite was poured into a beaker with distilled water and stirred for 5 minutes, then left to stand for 30 minutes, finally, the floating expanded perlite was taken out and dried in a vacuum drying oven at 120 °C for 48 h.

2.3 Preparation of LS–EP CPCM

In our previous study, the eutectic mass ratio of L–S was determined to be 82 : 18 by step-cooling curve experiments and DSC analysis.[32] The LS/EP CPCMs were synthesized using the vacuum impregnation process shown in Fig. 1.

First, L–S was compounded according to the mass ratio determined above, then different masses of L–S eutectics and purified EP were weighed (controlling the mass fraction of the L–S eutectics to be 60%, 65%, 70%, 75%, and 80%) into a beaker and stirred well. Then the beakers were put into a vacuum drying oven set to 80 °C 0.08 MPa for 6 hours, removing it every 2 h and stirring for 5 min. LS/EP CPCMs with mass fractions of 60%, 65%, 70%, 75%, and 80% L–S were synthesized.

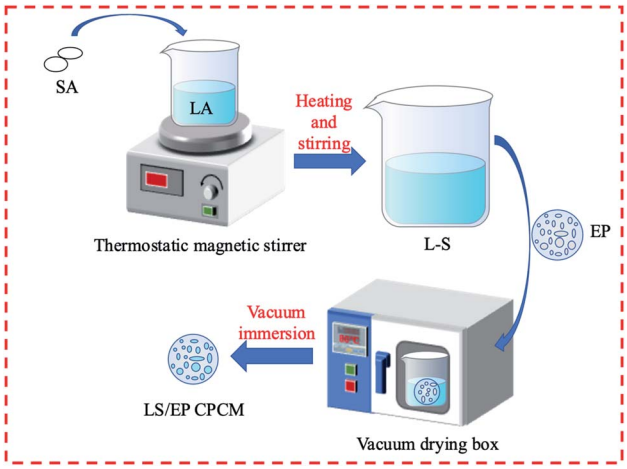

Fig. 1 Synthesis flow chart for LS/EP CPCMs.

2.4 Experimentation and characterization

2.4.1 Leakage experiments. The visual filter paper leakage circle method and the mass loss method were used to determine the maximum adsorption rate of PCM, using the following steps: (1) weighed 0.5 g of CPCM with different PCM mass fractions and spread it evenly on the filter paper in a 30 mm test area. (2) These filter papers were placed in a constant temperature drying oven at 80 °C for heat treatment for 2 hours. (3) The filter paper was removed from the oven and, after cooling to room temperature, the CPCM on the filter paper was moved to the balance for weighing; the mass loss of CPCM and the corresponding filter paper infiltration image were recorded at this time.

2.4.2 Properties characterization. Differential scanning calorimetry (DSC) was used to measure the phase change temperature and latent heat of the samples. The experimental conditions were set to 20–65 °C, 5 °C min^{-1}, and a nitrogen atmosphere. Scanning electron microscopy (SEM) was used to analyze the microscopic morphology of EP and LS/EP CPCM, and the working voltage was set to 20 kV. Thermogravimetric analysis (TGA) was used to analyze the thermal decomposition of the samples; the test temperature range was from 30 to 400 °C, with a heating rate of 10 °C min^{-1}, and a nitrogen flow rate of 100 ml min^{-1}. The crystal structure of the sample was characterized by X-ray diffraction (XRD), while the chemical structure was characterized by Fourier transform infrared spectroscopy (FT-IR).

2.4.3 Accelerated thermal cycling experiment. Reliability refers to the ability of the material to maintain its thermal properties and chemical structure during cycling. In practical engineering applications, the CPCM is in a phase change cycle

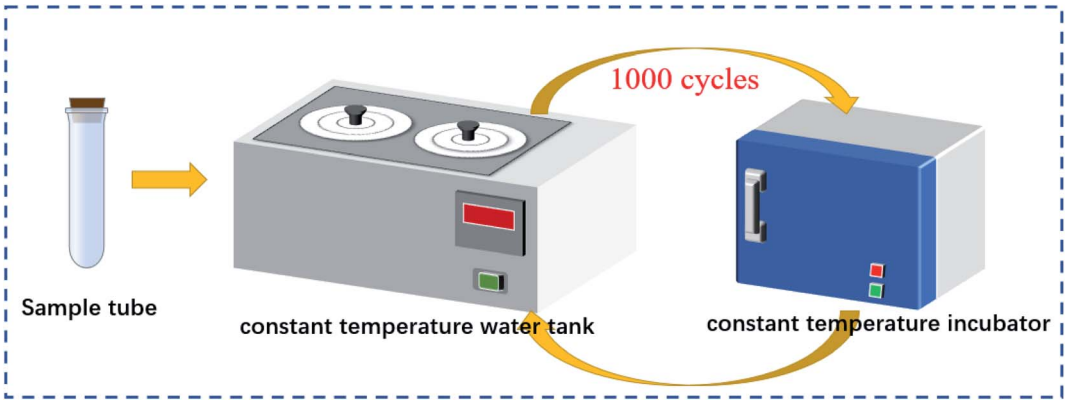

Fig. 2 Schematic diagram of the cycling experiment.

of continuous melting and solidification, so thermal reliability is particularly important. To analyze the reliability of the LS/EP CPCM, first, the samples were poured into marked test tubes, then the test tubes were put into a constant temperature water tank at 70 °C until the contents completely melted, then they were moved to a constant temperature incubator at 10 °C. After the contents had completely solidified, the tubes were moved to a constant temperature water tank at 70 °C, and this process was repeatedly cycled 1000 times. A schematic diagram of the cycling experiment is shown in Fig. 2. The phase change properties of the samples were tested after 250, 500, and 1000 cycles, and the chemical structure of the samples was characterized after 1000 cycles.

3. Results and discussion

3.1 Determination of maximum mass adsorption fraction

PCM is liquid at high temperature. If it is not effectively adsorbed in the pores of the EP, then it will flow onto the filter paper, which is the principle of the leak experiment. Therefore, leakage experiments were performed on LA-based CPCMs with mass fractions of 60%, 65%, 70%, 75%, and 80% L–S to determine the optimal mass fraction of L–S in the LS/EP CPCM. The corresponding filter paper leakage images are shown in Fig. 3, and the mass loss rates for each sample are shown in Table 1.

As can be seen from Fig. 3, for LS/EP, when the mass fraction of L–S is less than or equal to 70%, there is no trace of leakage on the filter paper. However, when the mass fraction of L–S is 75–80%, the filter paper has obvious leakage traces. Combined with the leakage fraction of LS/EP in Table 1, when the mass fraction of L–S is less than or equal to 70%, the leakage rate is controlled at 3%. Since L–S is a non-toxic and non-corrosive material, a little leakage is acceptable for building. In order to obtain an LS/EP CPCM with a larger latent heat, LS/EP with 70 wt% L–S was selected as the object of subsequent analysis.

Table 1 Mass of LS/EP CPCMs before and after heat treatment[a]

Material	L–S/%	M_b/g	M_a/g	Mass loss fraction/%
LS/EP	60	0.500	0.494	1.2
	65	0.500	0.493	1.4
	70	0.500	0.488	2.4
	75	0.500	0.472	5.6
	80	0.500	0.459	8.2

[a] M_b and M_a are the sample mass before and after heat treatment, respectively.

3.2 Analysis of SEM images

The SEM images of EP and LS/EP are shown in Fig. 4. It can be seen from Fig. 4(a) that the EP has a honeycomb-like pore structure as a whole, with a large number of irregular pores, which are not only interconnected but also communicate with the atmosphere. Therefore, it has sufficient space to adsorb the liquid PCM and suppress the leakage of the liquid PCM through some weak physical effects, such as capillary force. Fig. 4(b)

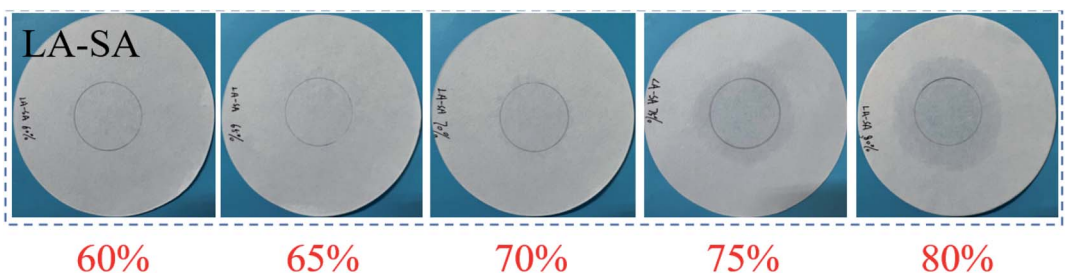

Fig. 3 Filter paper leakage images of LS/EP.

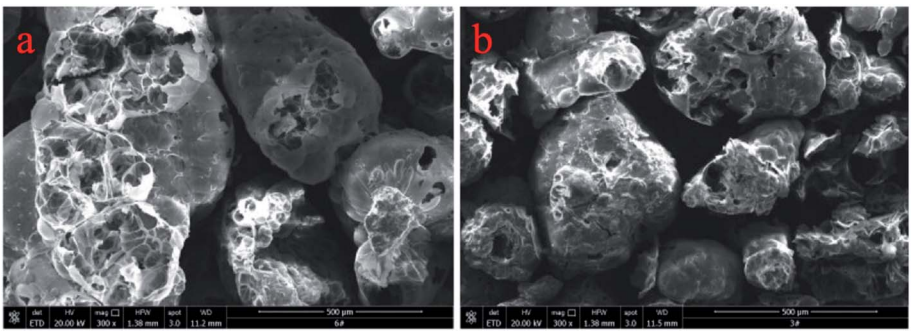

Fig. 4 SEM images of (a) EP and (b) LS/EP.

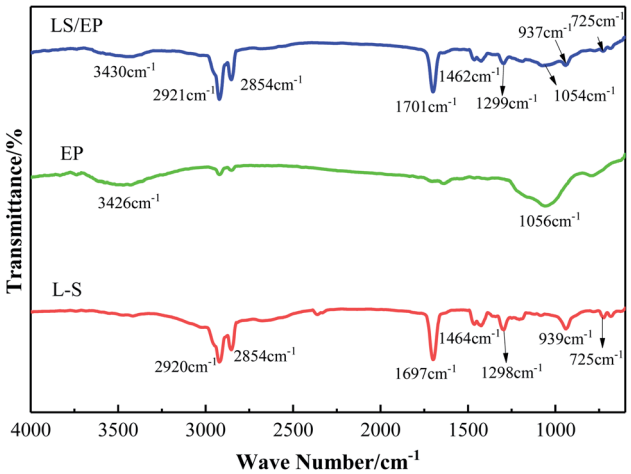

Fig. 5 FT-IR spectra of L–S, EP, and LS/EP.

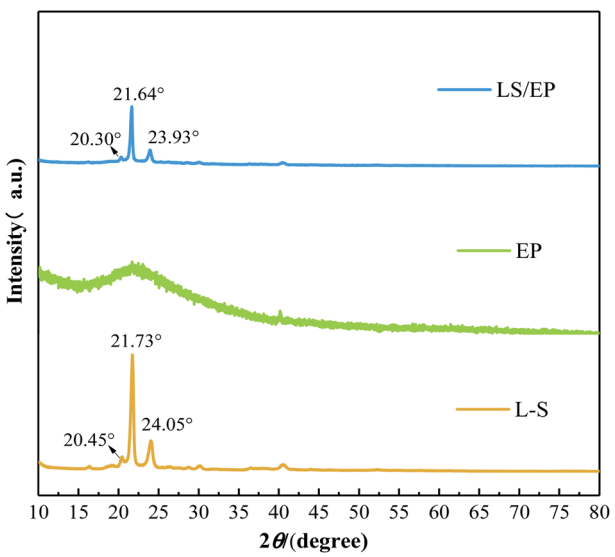

Fig. 6 XRD spectra for L–S, EP, and LS/EP.

shows the SEM image of LS/EP. Compared with the SEM images of EP, the pores are heavily reduced. This phenomenon indicates that the L–S eutectic PCM is adsorbed into the pores of the

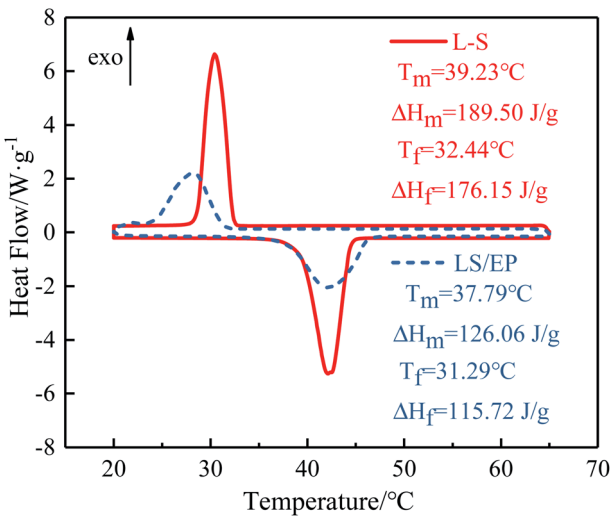

Fig. 7 DSC curves of L–S and LS/EP.

Table 2 Evaluation index data showing the latent heat performance of LA-based CPCMs

Materials	*R*/%	*E*/%	*μ*/%	*F*/%
LS/EP	66.62	66.12	99.25	95.17

EP. In addition, the outer contours of most of the pores are still clear, indicating that the mass fraction of the L–S determined by the leakage experiment is suitable. Therefore, by analyzing their micromorphology, it is concluded that EP can effectively adsorb L–S and prevent their leakage.

3.3 Chemical structure analysis

The chemical compatibility between EP and L–S was analyzed by FT-IR, and the corresponding FT-IR spectra are shown in Fig. 5. It can be found from Fig. 5 that two distinct characteristic absorption peaks appear in the FT-IR spectrum of EP. The absorption peaks at 3426 cm^{-1} and 1056 cm^{-1} correspond to the O–H stretching vibration and the Si–O–Si stretching vibration, respectively.

From Fig. 5, it is found that the FT-IR of L–S has different characteristic absorption peaks at 2920 cm^{-1}, 2854 cm^{-1},

Table 3 Comparison with other composites reported in the literature

CPCM	Melting temperature/°C	Latent heat/J g^{-1}	Reference
Stearic-capric acid/activated-attapulgite	21.8	72.6	35
Lauric acid/intercalated kaolinite	43.7	72.5	24
Lauric–palmitic–paraffin/expanded perlite	31.4	117.3	36
Lauric–myristic acid/porous wood flour	33.1	98.2	37
Capric–myristic acid/diatomite	22.75	67.03	38
Capric–stearic–palmitic acid/expanded graphite	25.39	140.22	16
Lauric–stearic acid/expanded perlite	37.79	126.06	This work

1697 cm^{-1}, 1464 cm^{-1}, 1298 cm^{-1} and 939 cm^{-1}. The wave numbers from large to small correspond to the asymmetric stretching vibration of $-CH_3$, symmetrical stretching vibration of $-CH_2$, stretching vibration of –C═O, bending vibration of $-CH_2$, in-plane bending vibration of –OH, out-of-plane deformation of–OH, and out-of-plane bending vibration of C–H bond. The FT-IR spectrum of LS/EP shows characteristic absorption peaks at 3430 cm^{-1}, 2921 cm^{-1}, 2854 cm^{-1}, 1701 cm^{-1}, 1462 cm^{-1}, 1299 cm^{-1}, 1054 cm^{-1} and 937 cm^{-1}; their wave numbers are very close to the characteristic absorption peaks in L–S and EP, and no new characteristic absorption peaks are generated. It is well known that chemical interactions between substances must create some new functional groups and atomic bonds. However, in the FT-IR analysis, no peaks disappeared or appeared in the FT-IR spectra of LS/EP compared to L–S and EP, indicating that no chemical reaction occurred during the preparation of LS/EP. Therefore, physical interaction is responsible for the LS/EP composite. Meanwhile, the SEM analysis results showed that L–S was absorbed into the pores of EP, indicating that the interaction between L–S and EP caused a capillary force.

3.4 Crystal structure analysis

The crystal structure of L–S, EP, and LS/EP CPCM was characterized using XRD to investigate whether the adsorption by the EP pore structure would destroy the crystal structure of L–S, and the results are shown in Fig. 6.

Table 4 Pyrolysis parameters of L–S and LS/EP CPCM

Material	Decomposition temperature/°C			
	Initial	Fastest	End	Mass loss fraction/%
EP	—	—	—	0
L–S	110.08	241.19	276.25	98.63
LS/EP	132.20	218.15	255.38	67.33

It can be seen from Fig. 6 that the diffraction intensity of EP is low, and it has no crystal peaks, indicating that EP is an amorphous material. In addition, it can be seen that L–S has strong diffraction peaks at 20.45°, 21.73°, and 24.05°. LS/EP also showed strong diffraction peaks near these diffraction angles, corresponding to 20.30°, 21.64°, and 23.93°, and no new diffraction peaks were generated. Based on the above analysis, it is not difficult to see that the adsorption of EP did not destroy the crystal structure of L–S, and no new crystal phase was generated by chemical reaction during the synthesis process. Moreover, the diffraction peaks of LS/EP CPCM shifted to a small angle and the diffraction intensity decreased compared with L–S, indicating that there is a physical interaction between

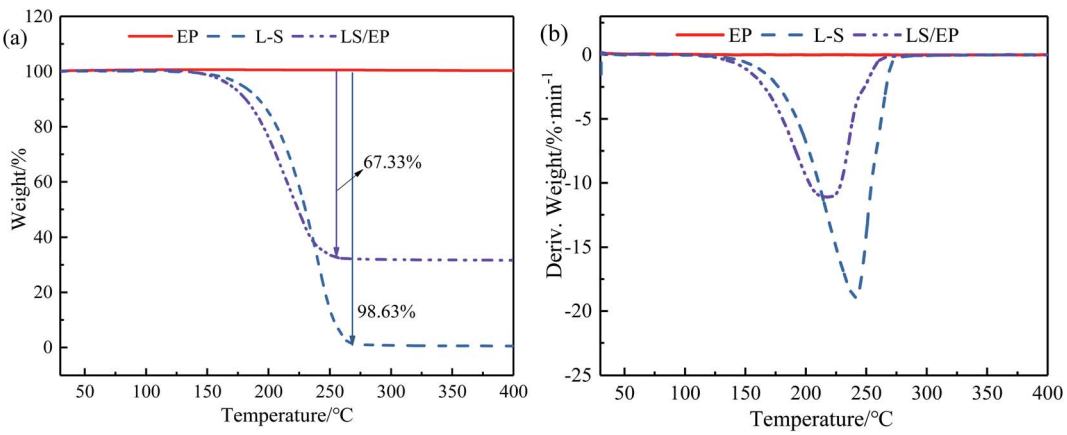

Fig. 8 (a) TG and (b) DTG curves for EP, L–S, and LS/EP.

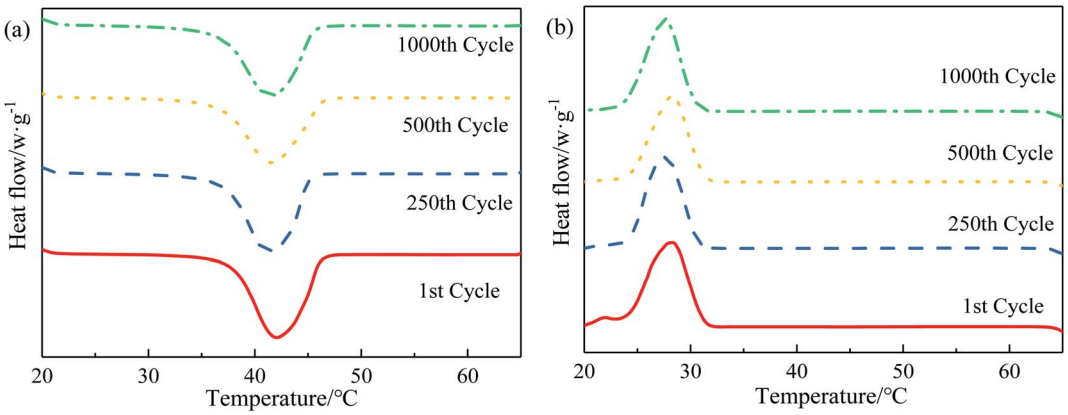

Fig. 9 DSC curves after several cycles: (a) melting process of LS/EP. (b) Solidification process of LS/EP.

L–S and EP, which increases the interlayer distance and reduces the crystallinity of L–S.

3.5 Phase change properties analysis

The DSC curves of L–S and LS/EP are shown in Fig. 7. As shown in Fig. 7, comparing the peak shapes and positions of the L–S and LS/EP, it is found that they all have a single endothermic and exothermic peak, and the L–S and LS/EP have a high coincidence in the temperature range of endothermic and exothermic peaks, which indicates that the latent heat of LS/EP comes from L–S. Their phase change parameters are described in detail below.

From Fig. 7, it can be seen that the melting temperatures of L–S and LS/EP are 39.23 °C and 37.79 °C, and the latent heats are 189.50 J g^{-1} and 126.06 J g^{-1}; the solidification temperatures are 32.44 °C and 31.29 °C, and the latent heats are 176.15 J g^{-1} and 115.72 J g^{-1}. Detailed analysis of the above data shows that, compared with L–S, the phase change temperatures of LS/EP CPCM decreased, which is due to the pore structure of EP dividing the originally integrated fatty acid molecules into several small parts, increasing the heat transfer area and improving the sensitivity to thermal stimulation. In addition,

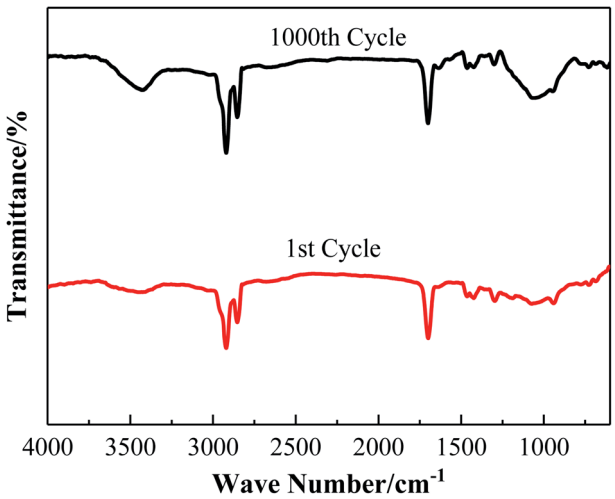

Fig. 11 FT-IR spectra of LS/EP before and after cycling.

the latent heat performance of the LS/EP CPCM can be effectively evaluated by four indices: effective adsorption rate (R), effective heat storage and release percentage (E), relative heat

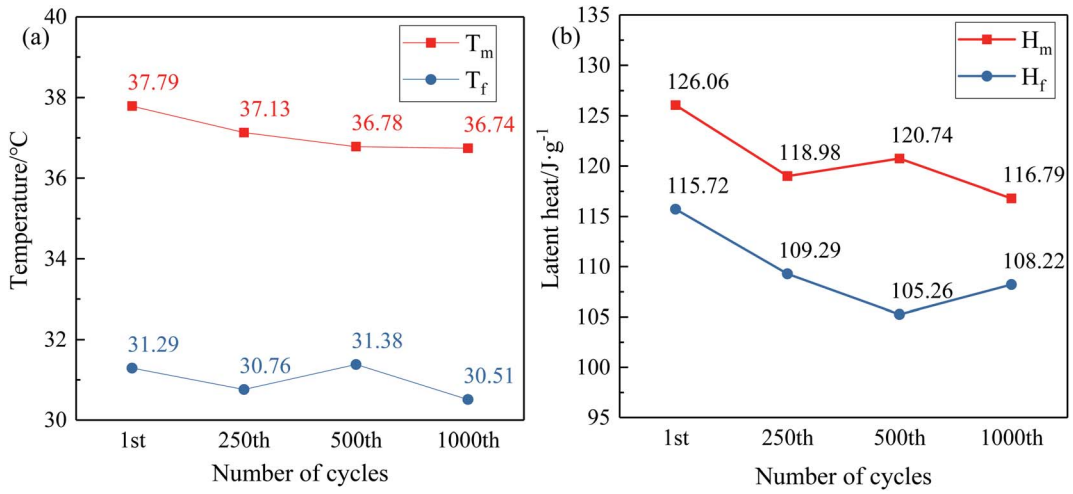

Fig. 10 The change trend of (a) phase change temperature and (b) latent heat of LS/EP during cycles.

storage efficiency (μ), and crystallinity (F). The calculation method is shown in eqn (1)–(4),[33,34] and the calculation results are shown in Table 2.

$$R = \frac{H_{m,CPCM}}{H_{m,PCM}} \times 100\% \quad (1)$$

$$E = \frac{H_{m,CPCM} + H_{f,CPCM}}{H_{m,PCM} + H_{f,PCM}} \times 100\% \quad (2)$$

$$\mu = \frac{E}{R} \times 100\% \quad (3)$$

$$F = \frac{R}{\omega} \times 100\% \quad (4)$$

where $H_{m,CPCM}$ and $H_{f,CPCM}$ refer to the latent heat of melting and freezing of LS/EP, respectively; $H_{m,PCM}$ and $H_{f,PCM}$ refer to the latent heat of melting and freezing of L–S eutectics, respectively; ω refers to the optimal mass fraction of L–S.

According to Table 2, the effective adsorption rate (R) of LS/EP is 66.62% and the effective heat storage and release percentage (E) is 66.12%, which are slightly lower than the actual incorporation rate in the leakage experiment, but within the allowable error range, indicating that the leakage experiment designed in this work can accurately determine the optimal mass fraction of PCM. Furthermore, the relative thermal storage efficiency (μ) of LS/EP is 99.25%, which is higher than 98%. This means that almost all of the L–S in LS/EP can effectively complete the endothermic and exothermic phase change cycle. Crystallinity is an indicator of the degree of crystallization of PCM: the higher the crystallinity, the smaller the latent heat loss. In this work, the crystallinity (F) of the prepared LS/EP is higher than 95%, indicating that the pore structure of EP has little effect on the latent heat of L–S. The above data show that the prepared LS/EP has excellent phase change properties in terms of four aspects, R, E, μ, and F.

In addition, as shown in Table 3, we compared the latent heat of LS/EP with other composites reported in the literature. The latent heat of the synthesized LS/EP is larger than that of many clay-based CPCMs, but a little smaller than that of carbon-based CPCMs, such as capric–stearic–palmitic acid/expanded graphite.[16] However, carbon-based CPCMs are more costly. Therefore, the prepared LS/EP is a more economical option for construction materials.

3.6 Thermal stability

To investigate the thermal stability of L–S and LS/EP and the internal relationship between them, we used thermogravimetric analysis (TGA) to analyze the thermal decomposition situation of L–S and LS/EP CPCM. The results are shown in Fig. 8 and Table 4.

It can be seen from Fig. 8 that the TG and DTG curves of EP both are a horizontal straight line, indicating that EP has good thermal stability below 400 °C. The initial decomposition temperatures of L–S and LS/EP are 110.08 °C and 132.20 °C, the fastest decomposition temperatures are 241.19 °C and 218.15 °C, and the end decomposition temperatures are 276.25 °C and 255.38 °C. Meanwhile, the mass loss rate of LS/EP is 67.33%, which is very close to the adsorption rate of L–S in the leakage experiments. This phenomenon demonstrates that the mass loss of LS/EP is caused by the decomposition of L–S in the composite. Overall, the initial decomposition temperature of LS/EP CPCM is much higher than the maximum temperature occurring in the building envelope, indicating that LS/EP CPCM has excellent thermal stability as a building material.

3.7 Reliability

3.7.1 Thermal reliability. Building materials work in an alternating temperature environment. Large changes in the phase change temperature and latent heat of materials during thermal cycling can negatively affect the engineering applications of materials. Many scholars have performed accelerated phase change cycles on CPCMs to investigate their thermal reliability and a small variation of phase change parameters is considered acceptable.[16,24,35,39] In this work, the synthesized LS/EP was subjected to 1000 accelerated phase change cycles and the phase change properties of LS/EP were characterized *via* DSC after 1, 250, 500 and 1000 cycles. The variation of phase change parameters within 10% was considered acceptable. The DSC curves are shown in Fig. 9 and the corresponding phase change parameter trends of change are shown in Fig. 10.

Observe the DSC curves of LS/EP in Fig. 9; as the accelerated phase change cycle proceeds, the peak shape and number of the endothermic peaks remain unchanged, and only the area of the endothermic peaks changes slightly. Furthermore, according to the data in Fig. 10, after 250, 500 and 1000 cycles, the melting temperature of LS/EP changed from 37.79 °C to 37.13 °C, 36.78 °C, and 36.74 °C, decreasing by 0.66 °C, 1.01 °C, and 1.05 °C, respectively. The latent heat decreased from 126.06 J g^{-1} to 118.98 J g^{-1}, 120.74 J g^{-1}, and 116.79 J g^{-1}, and decreased by 7.08 J g^{-1}, 5.32 J g^{-1}, and 9.27 J g^{-1}. It can be seen that after 1000 cycles, the relative change rate of the melting temperature of LS/EP does not exceed 3%, and the relative change rate of latent heat does not exceed 8%. Therefore, LS/EP has good thermal reliability and it still has a suitable phase change temperature and a high level of latent heat after cycling for the construction field.

3.7.2 Chemical reliability. In terms of chemical reliability, comparing the FT-IR spectra of LS/EP before and after cycling in Fig. 11, it is not difficult to find that neither the peak shape nor the absorption band of the functional groups were changed during cycling, and no new characteristic absorption peaks were generated, indicating that LS/EP has good chemical reliability.

4. Conclusions

In this work, L–S used as a PCM was compounded with EP *via* vacuum adsorption to synthesize LS/EP CPCMs. The maximum mass adsorption rate of the PCM, microscopic morphology, chemical and crystal structure, phase change properties, thermal stability, and reliability of LS/EP were characterized using leak tests, SEM, FT-IR, XRD, DSC, TG, and accelerated

phase change cycling experiments. The following conclusions are obtained:

(1) The maximum mass adsorption rate of EP on L–S is 70%. Under this adsorption rate, SEM images show that L–S is uniformly distributed in the pores of EP.

(2) The FT-IR and XRD patterns showed that EP is chemically compatible with L–S, and the addition of EP did not destroy the original crystal structure of L–S.

(3) The melting temperature of LS/EP is 37.79 °C, with a latent heat of melting of 126.05 J g^{-1}, and LS/EP has a crystallinity of over 90%. TG analysis showed that LS/EP does not undergo thermal decomposition in the construction field.

(4) The results of accelerated phase change cycling experiments showed that the phase change temperature of LS/EP changes by less than 3% and the latent heat changed by less than 8% after 1000 cycles, and no new characteristic absorption peaks were generated, so the LS/EP has good reliability.

Conflicts of interest

There are no conflicts to declare.

Acknowledgements

This work was supported by financial assistance from Jiangxi Provincial Department of Education Science and Technology Research Project (GJJ200830) and Jiangxi University of Science and Technology High-level Talents Research Start-up Project (2021205200100553).

References

1 T. Jiang, S. Li, Y. Yu and Y. Peng, Energy-related carbon emissions and structural emissions reduction of China's construction industry: the perspective of input–output analysis, *Environ. Sci. Pollut. Res.*, 2022, 1–13.

2 R. W. Apeaning, Technological constraints to energy-related carbon emissions and economic growth decoupling: a retrospective and prospective analysis, *J. Cleaner Prod.*, 2021, **291**, 125706.

3 Tsinghua University Building Energy Conservation Research Center, *Annual Development Research Report of Building Energy Efficiency in China 2020*, China Construction Industry Press, Beijing, 2020.

4 S. Raoux, Phase change materials, *Annu. Rev. Mater. Res.*, 2009, **39**, 25–48.

5 Y. Dutil, D. R. Rousse, N. B. Salah, S. Lassue and L. Zalewski, A review on phase-change materials: mathematical modeling and simulations, *Renewable Sustainable Energy Rev.*, 2011, **15**(1), 112–130.

6 F. Kuznik, D. David, K. Johannes and J.-J. Roux, A review on phase change materials integrated in building walls, *Renewable Sustainable Energy Rev.*, 2011, **15**(1), 379–391.

7 D. Zhou, C.-Y. Zhao and Y. Tian, Review on thermal energy storage with phase change materials (PCMs) in building applications, *Appl. Energy*, 2012, **92**, 593–605.

8 M. Song, F. Niu, N. Mao, Y. Hu and S. Deng, Review on building energy performance improvement using phase change materials, *Energ. Build.*, 2018, **158**, 776–793.

9 H. A. Hattan, M. Madhkhan and A. Marani, Thermal and mechanical properties of building external walls plastered with cement mortar incorporating shape-stabilized phase change materials (SSPCMs), *Constr. Build. Mater.*, 2021, **270**, 121385.

10 A. Louanate, R. E. Otmani, K. Kandoussi, M. H. Boutaous and D. Abdelmajid, Energy saving potential of phase change materials-enhanced building envelope considering the six Moroccan climate zones, *J. Build. Phys.*, 2021, 17442591211006444.

11 K. Yu, Y. Liu and Y. Yang, Review on form-stable inorganic hydrated salt phase change materials: preparation, characterization and effect on the thermophysical properties, *Appl. Energy*, 2021, **292**, 116845.

12 L. Liu, J. Li, Y. Deng, Z. Yang, K. Huang and S. Zhao, Optimal design of multi-layer structure composite containing inorganic hydrated salt phase change materials and cement: lab-scale tests for buildings, *Constr. Build. Mater.*, 2021, **275**, 122125.

13 M. M. Umair, Y. Zhang, K. Iqbal, S. Zhang and B. Tang, Novel strategies and supporting materials applied to shape-stabilize organic phase change materials for thermal energy storage–a review, *Appl. Energy*, 2019, **235**, 846–873.

14 X. Tong, N. Li, M. Zeng and Q. Wang, Organic phase change materials confined in carbon-based materials for thermal properties enhancement: recent advancement and challenges, *Renewable Sustainable Energy Rev.*, 2019, **108**, 398–422.

15 Y. Yuan, N. Zhang, W. Tao, X. Cao and Y. He, Fatty acids as phase change materials: a review, *Renewable Sustainable Energy Rev.*, 2014, **29**, 482–498.

16 W. Du, H. Fei, Y. Pan, Q. He, J. Zhou and X. Liang, Development of capric acid-stearic acid-palmitic acid low-eutectic phase change material with expanded graphite for thermal energy storage, *Constr. Build. Mater.*, 2022, **320**, 126309.

17 C. Cárdenas-Ramírez, M. A. Gómez and F. Jaramillo, Comprehensive analysis of the thermal properties of capric-myristic, lauric-myristic and palmitic-stearic acids and their shape-stabilization in an inorganic support, *J. Energy Storage*, 2021, **34**, 102015.

18 Y. He, X. Zhang, Y. Zhang, Q. Song and X. Liao, Utilization of lauric acid-myristic acid/expanded graphite phase change materials to improve thermal properties of cement mortar, *Energ. Build.*, 2016, **133**, 547–558.

19 X. Xiao, P. Zhang and M. Li, Preparation and thermal characterization of paraffin/metal foam composite phase change material, *Appl. Energy*, 2013, **112**, 1357–1366.

20 W. Li, Z. Qu, B. Zhang, K. Zhao and W. Tao, Thermal behavior of porous stainless-steel fiber felt saturated with phase change material, *Energy*, 2013, **55**, 846–852.

21 Z. Zhang and X. Fang, Study on paraffin/expanded graphite composite phase change thermal energy storage material, *Energy Convers. Manage.*, 2006, **47**(3), 303–310.

22 G. Fang, H. Li, Z. Chen and X. Liu, Preparation and characterization of stearic acid/expanded graphite composites as thermal energy storage materials, *Energy*, 2010, **35**(12), 4622–4626.

23 T. Qian, J. Li and Y. Deng, Pore structure modified diatomite-supported PEG composites for thermal energy storage, *Sci. Rep.*, 2016, **6**(1), 1–14.

24 S. Song, L. Dong, Y. Zhang, S. Chen, Q. Li, Y. Guo, S. Deng, S. Si and C. Xiong, Lauric acid/intercalated kaolinite as form-stable phase change material for thermal energy storage, *Energy*, 2014, **76**, 385–389.

25 P. Lv, M. Ding, C. Liu and Z. Rao, Experimental investigation on thermal properties and thermal performance enhancement of octadecanol/expanded perlite form stable phase change materials for efficient thermal energy storage, *Renewable energy*, 2019, **131**, 911–922.

26 D.-c. Gao, Y. Sun, A. M. Fong and X. Gu, Mineral-based form-stable phase change materials for thermal energy storage: a review on encapsulation techniques, performance enhancements and practical applications, *Energy Storage Mater.*, 2022, **46**, 100–128.

27 Y. Bian, K. Wang, J. Wang, Y. Yu, M. Liu and Y. Lv, Preparation and properties of capric acid: stearic acid/hydrophobic expanded perlite-aerogel composite phase change materials, *Renewable Energy*, 2021, **179**, 1027–1035.

28 S. Hasanabadi, S. M. Sadrameli and S. Sami, Preparation, characterization and thermal properties of surface-modified expanded perlite/paraffin as a form-stable phase change composite in concrete, *J. Therm. Anal. Calorim.*, 2021, **144**(1), 61–69.

29 S. Zhang, D. Feng, L. Shi, L. Wang, Y. Jin, L. Tian, Z. Li, G. Wang, L. Zhao and Y. Yan, A review of phase change heat transfer in shape-stabilized phase change materials (ss-PCMs) based on porous supports for thermal energy storage, *Renewable Sustainable Energy Rev.*, 2021, **135**, 110127.

30 H. Xiong, K. Yuan, J. Xu and M. Wen, Pore structure, adsorption, and water absorption of expanded perlite mortar in external thermal insulation composite system during aging, *Cem. Concr. Compos.*, 2021, **116**, 103900.

31 A. Sarı and A. Karaipekli, Preparation, thermal properties and thermal reliability of capric acid/expanded perlite composite for thermal energy storage, *Mater. Chem. Phys.*, 2008, **109**(2–3), 459–464.

32 Z. Fan, Y. Zhao, X. Liu, Y. Shi and D. Jiang, Thermal Properties and Reliabilities of Lauric Acid-Based Binary Eutectic Fatty Acid as a Phase Change Material for Building Energy Conservation, *ACS Omega*, 2022, **7**(18), 16097–16108.

33 Y. Luo, S. Xiong, J. Huang, F. Zhang, C. Li, Y. Min, R. Peng and Y. Liu, Preparation, characterization and performance of paraffin/sepiolite composites as novel shape-stabilized phase change materials for thermal energy storage, *Sol. Energy Mater. Sol. Cells*, 2021, **231**, 111300.

34 T. Qian, J. Li, X. Min, W. Guan, Y. Deng and L. Ning, Enhanced thermal conductivity of PEG/diatomite shape-stabilized phase change materials with Ag nanoparticles for thermal energy storage, *J. Mater. Chem. A*, 2015, **3**(16), 8526–8536.

35 S. Song, L. Dong, S. Chen, H. Xie and C. Xiong, Stearic–capric acid eutectic/activated-attapulgiate composite as form-stable phase change material for thermal energy storage, *Energy Convers. Manage.*, 2014, **81**, 306–311.

36 Z. Fan, Y. Zhao, X. Liu, Y. Shi and D. Jiang, Development of a new composite material for building energy storage based on lauric acid-palmitic acid-paraffin ternary eutectic and expanded perlite, *J. Energy Storage*, 2022, **53**, 105136.

37 L. Ma, C. Guo, R. Ou, L. Sun, Q. Wang and L. Li, Preparation and characterization of modified porous wood flour/lauric-myristic acid eutectic mixture as a form-stable phase change material, *Energy Fuels*, 2018, **32**(4), 5453–5461.

38 L. Fu, F. Dong, P. He and Y. Yang, Study on preparation and properties of capric-myristic acid/diatomite form-stable phase change energy storage materials, *J. Funct. Mater.*, 2013, **44**(10), 1465–1468.

39 Z. Fan, Y. Zhao, X. Liu, Y. Shi and D. Jiang, Thermal properties and reliabilities of myristic acid–paraffin wax binary eutectic mixture as a phase change material for solar energy storage, *RSC Adv.*, 2022, **12**(20), 12303–12309.